Supporting Information

Woodhead et al. 10.1073/pnas.1218462110

SI Materials and Methods

Three-Dimensional Reconstruction Procedure. Three-dimensional reconstruction of scallop filaments was carried out using a modified single-particle approach. Initially, we used the iterative helical real space reconstruction (IHRSR) technique (1), in which filament images are computationally cut into short segments, which are matched against projections of a model with the correct symmetry, rotated about the filament axis at 4° intervals. The angle of best match determined by correlation methods is used in computing backprojections of the images to provide a 3D reconstruction, which is then helically averaged. This reconstruction is used as a new model, and the process is iterated until there is no further change in the reconstruction. This approach was straightforward for negatively stained scallop filaments and gave a 3D reconstruction with ~6-nm resolution, similar in appearance to published reconstructions based on negative staining (2, 3) (Fig. S4*A*).

However, the same procedure failed with unstained, frozen-hydrated filaments. The high level of symmetry (sevenfold rotational symmetry), together with the high intrinsic noise and low contrast of the images, caused the projection matching to fail, as many of the different views of the segments looked very similar to each other. In addition, the subfilament structure of the backbone tended to dominate the projections so that head alignment was compromised. We therefore used a different approach. Using knowledge of their symmetry (2, 4, 5), it is possible to compute reconstructions of individual filaments by a modified IHRSR procedure. Backprojection angles are assigned to each segment based on this known symmetry rather than on projection matching to a model. Reconstructions of individual half-filaments were computed in this way and helically averaged. The resulting reconstructions were aligned in Chimera, and then averaged in SPIDER (using the Chimera alignment parameters) to generate a final reconstruction.

Reconstruction Statistics and Resolution. The reconstruction was based on the 16 best filament halves (chosen from a total of 279), each containing an average of 25 segments, 72-nm (i.e., five crowns) long. Individual segments used in the reconstruction were staggered by 14.4 nm (one crown); thus, ~25 + 5 = 30 unique crowns (=210 unique motifs due to sevenfold symmetry) were averaged per half-filament. The total number of unique motifs used in the reconstruction was therefore ~3,360. The reconstruction had a resolution of ~5 nm according to the Fourier shell correlation using a 0.5 threshold. This is comparable to the resolution obtained in a previous scallop filament cryo-reconstruction (5) and similar to the highest resolution myosin reflections reported in X-ray diffraction patterns of living scallop muscle (4, 6), suggesting substantial mobility of the myosin heads in this muscle in vivo (5). Thus, the limited resolution of the reconstruction appears to reflect intrinsic motions of the heads rather than problems of specimen preparation, imaging, or reconstruction (5). The power spectrum of the reconstruction filtered to this resolution is similar to the averaged power spectrum of the filament images used in the reconstruction and to the myosin component of the X-ray patterns (Fig. S2), supporting the validity of the reconstruction.

Atomic Fitting. Although the resolution of the reconstruction was relatively limited, atomic fitting was substantially constrained by the requirement of fitting multiple asymmetric motifs within the helical tracks. Fitting was carried out in two stages. The volume and shape of the head-pair motif in the reconstruction was broadly similar to those of the interacting-head structure in the smooth muscle heavy meromyosin and tarantula filament models [Protein Data Bank (PDB) ID codes 1I84 and 3DTP, respectively]; the main density was along the top of the motif and must therefore represent the MDs of the two heads. A good fit to this region of the motif was obtained for the two motor domains linked as a single rigid body, using both the smooth muscle and tarantula models, with tarantula giving the better fit of the two. Tarantula also gave the better fit when the two regulatory domains were fitted to the motif as a single rigid body, separate from the motor domains. However, the best fit for the combined motor domains was not compatible with the best fit for the combined regulatory domains without significant modification. This precluded a good global fit into the motif for either of the complete atomic models (i.e., including all four domains as a single rigid body). We therefore first fitted the two tarantula motor domains as a single rigid body, and then each of the regulatory domains as individual rigid bodies, to obtain an overall initial best fit. In addition to the boundaries imposed by the density envelope of the reconstruction, each regulatory domain was constrained so that the N terminal of the heavy chain remained adjacent to the C terminal of its corresponding motor domain heavy chain. The approximate fit obtained in this way with the tarantula structure was used as a template for initial alignment of the relaxed state (prepower stroke) scallop atomic model for the motor domains derived from scallop S1.ADP.Vi (PDB ID code 1QVI) (7) truncated at heavy chain residue Met-773 [within the pliant point region, where significant flexibility has been reported (8)]. The regulatory domain of this structure was not used because the S1 had been crystallized in the presence of Ca^{2+} and the regulatory domain may therefore have had a different conformation from that in the relaxed state. Instead, an atomic model of the Ca^{2+}-free scallop regulatory domain (PDB ID code 3JTD) (9) was used to replace the regulatory domains in the fitted tarantula model. [Indeed, when the ELC region of 1QVI (containing Ca^{2+} bound to the ELC) was superimposed on the tarantula template, the N-terminal domain of the RLC projected out of the density envelope. When the Ca^{2+}-free (off-state) RD (3JTD) ELC region was superimposed over the Ca^{2+}-bound RD, the RLC was then found to stay within the density envelope, consistent with the expectation that an ADP.Vi MD/Ca^{2+}-free RD model should give the best fit to the relaxed filament.] Both the motor and regulatory domain models were then readjusted within the density envelope to achieve the best final fit while retaining correct heavy chain continuity between regulatory and motor domains within each head. Finally, the remaining density joining the two S1 regions to the filament backbone was fitted with an atomic model of the N-terminal region of scallop myosin S2 (PDB ID code 3BAS) (10) while ensuring that the C-terminal heavy chain truncation points were in close proximity at the head–rod junction.

1. Egelman EH (2000) A robust algorithm for the reconstruction of helical filaments using single-particle methods. *Ultramicroscopy* 85(4):225–234.

2. Vibert P, Craig R (1983) Electron microscopy and image analysis of myosin filaments from scallop striated muscle. *J Mol Biol* 165(2):303–320.

3. AL-Khayat HA, Morris EP, Squire JM (2009) The 7-stranded structure of relaxed scallop muscle myosin filaments: Support for a common head configuration in myosin-regulated muscles. *J Struct Biol* 166(2):183–194.
4. Wray JS, Vibert PJ, Cohen C (1975) Diversity of cross-bridge configurations in invertebrate muscles. *Nature* 257(5527):561–564.
5. Vibert P (1992) Helical reconstruction of frozen-hydrated scallop myosin filaments. *J Mol Biol* 223(3):661–671.
6. Millman BM, Bennett PM (1976) Structure of the cross-striated adductor muscle of the scallop. *J Mol Biol* 103(3):439–467.
7. Gourinath S, et al. (2003) Crystal structure of scallop myosin S1 in the pre-power stroke state to 2.6 Å resolution: Flexibility and function in the head. *Structure* 11(12):1621–1627.
8. Houdusse A, Szent-Györgyi AG, Cohen C (2000) Three conformational states of scallop myosin S1. *Proc Natl Acad Sci USA* 97(21):11238–11243.
9. Himmel DM, Mui S, O'Neall-Hennessey E, Szent-Györgyi AG, Cohen C (2009) The on-off switch in regulated myosins: Different triggers but related mechanisms. *J Mol Biol* 394(3):496–505.
10. Brown JH, et al. (2008) An unstable head-rod junction may promote folding into the compact off-state conformation of regulated myosins. *J Mol Biol* 375(5):1434–1443.

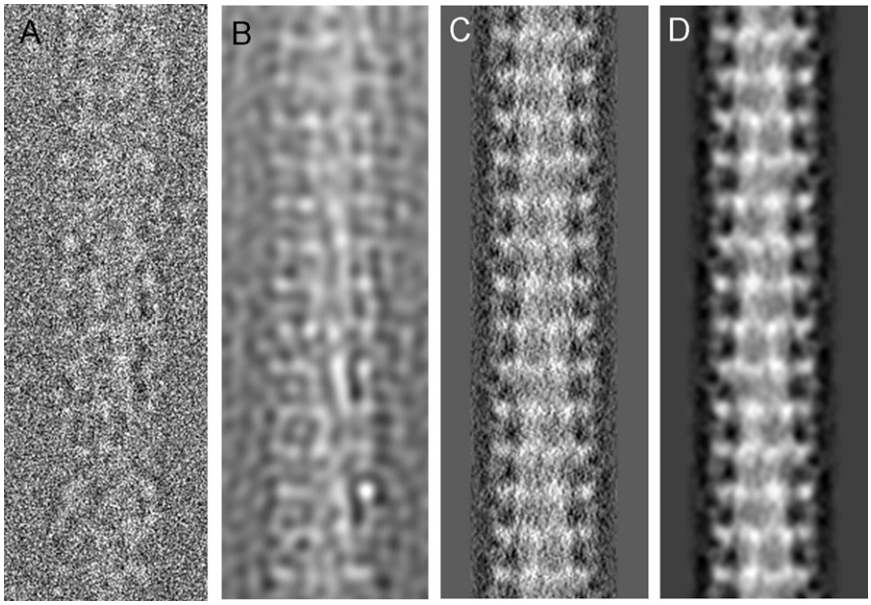

Fig. S1. Comparison of reconstruction with filament images. (*A*) Raw image at 4.6-μm defocus; (*B*) same as *A* but with high-frequency noise removed by Fourier filtration; (*C*) projection of reconstruction; (*D*) same as *C* but Fourier filtered to ∼5-nm resolution. The features in the final reconstruction are consistent with the original images (cf. also Fig. S2). *A* and *B* are in reverse contrast (protein white) for consistency with *C* and *D*.

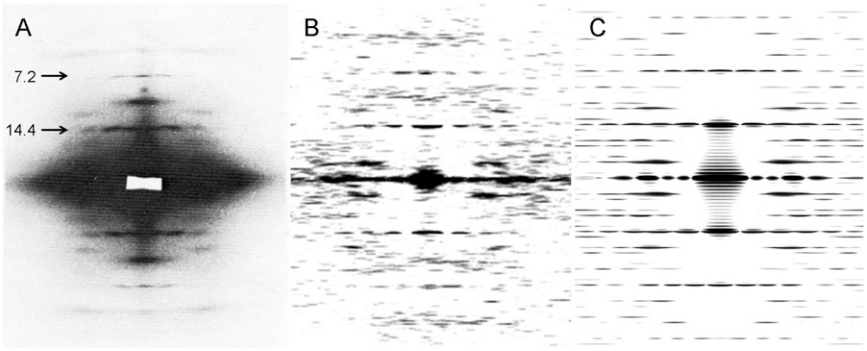

Fig. S2. Comparison of X-ray diffraction pattern of live scallop muscle (*A*) (1) with power spectra of the filaments used in reconstruction (*B*) and of the reconstruction itself (*C*). The computed intensities from the filaments agree well in axial and radial position with those from the X-ray pattern (Table S1), implying good preservation of native structure in the cryo-EM images. The good correspondence between the patterns in *B* and *C* supports the validity of the reconstruction. The arrows indicate 14.4- and 7.2-nm reflections. *A* was originally published in *Nature*. Reprinted by permission from Macmillan Publishers Ltd: *Nature* (1), Copyright (1975).

1. Wray JS, Vibert PJ, Cohen C (1975) Diversity of cross-bridge configurations in invertebrate muscles. *Nature* 257(5527):561–564, http://www.nature.com/nature/index.html.

Fig. S3. Position of S2 in the reconstruction, showing relationship to actin-binding cleft on blocked MD (colors as in Fig. 2*B*).

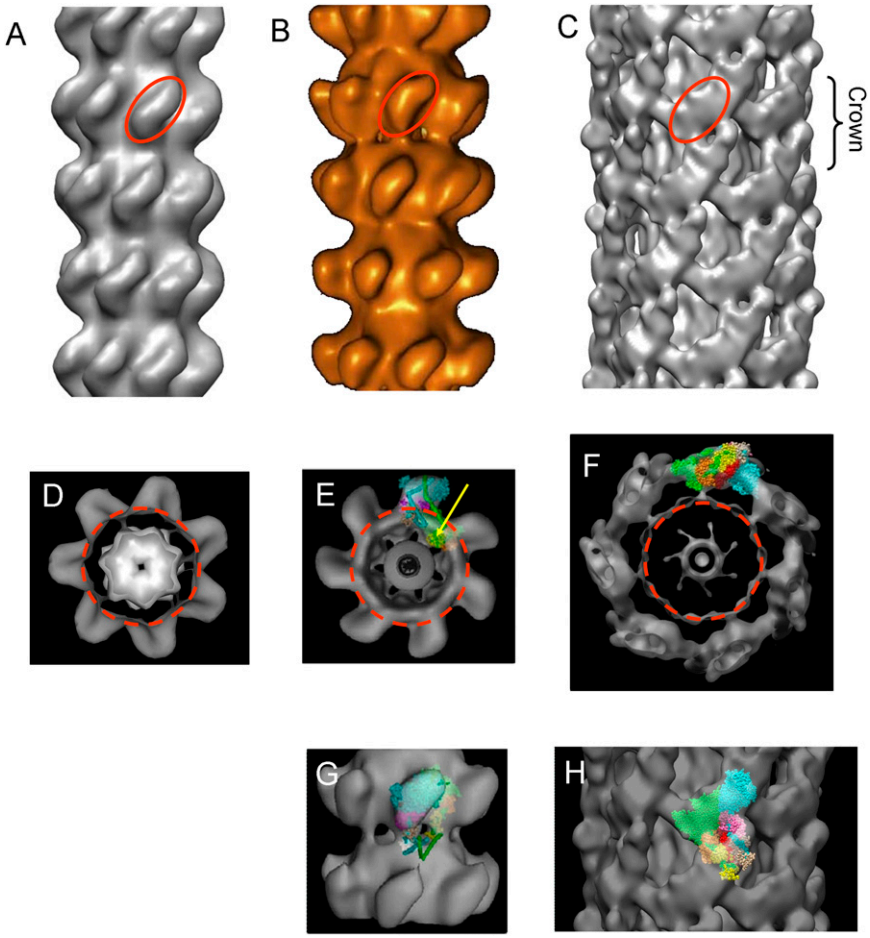

Fig. S4. Reconciling the reconstruction with previous scallop thick-filament reconstructions. Longitudinal (*A*–*C*, *G*, and *H*) and transverse (*D*–*F*) views of negative stain (*A*, *B*, *D*, *E*, and *G*) and cryo (*C*, *F*, and *H*) reconstructions, all on same scale. Bare zone up in *A*–*C*, *G*, and *H*; looking toward bare zone in *D*–*F*. The first reconstruction of scallop thick filaments (using negative staining combined with helical reconstruction methods) revealed a right-handed, helical organization of elongated motifs with sevenfold rotational symmetry (1). We (*A*) and AL-Khayat et al. [*B* (2)] obtained similar negative stain reconstructions to (1) using single-particle techniques. Comparison with the cryo-reconstruction (*C* and *H*) suggests that the repeating motif in the negative stain structures (red oval) corresponds only to the combined motor domains of the two heads (the strongest feature of the cryo-reconstruction) and that the weaker regulatory domains are not visualized. In the negative stain reconstructions, the heads appear to fuse with the backbone [*A*, *B*, *D*, and *E* (1, 2)], whereas in the cryo-reconstruction, they lie in a shell above it [*F* (3)]. This suggests that the heads collapse on to the backbone during the staining procedure, although there appears to be little shrinkage of the backbone itself (red circle in *D*–*F*). This collapse is reflected in a smaller filament diameter in the negative stain compared with the cryo-reconstructions (compare *A*, *B*, *D*, and *E*, with *C* and *F*), and in the original images [37-nm diameter in negative stain compared with 42-nm by cryo (4)]. In the negative stain reconstructions, detail is insufficient to resolve individual myosin heads [*A*, *B*, *D*, and *E* (1)], making interpretation of their organization highly speculative [resolution in ref. 1 is 7 nm and in ref. 2 is 6.5 nm (according to Fourier shell correlation 0.5 criterion)]. In ref. 1, it was suggested that the heads lay parallel to each other pointing away from the bare zone. In ref. 2, the structure was interpreted in terms of the interacting-head atomic model (5), but one of the heads (the blocked head) was placed at very low radius, where it would be inside the filament backbone (yellow arrow in *E*); in addition, there are no apparent intermolecular contacts along the long-pitch helices. We find that both heads are positioned above the backbone, oriented very differently from those in ref. 2 (compare *G* with *H*) and make multiple contacts along the helices. In the previous cryo-EM study of scallop filaments (3), it was concluded that the heads had different conformations from each other and were splayed apart axially. However, the reconstruction did not unambiguously define the two heads and was carried out before myosin head atomic structures were available, precluding definitive interpretation. Analysis of our reconstruction shows that the apparent splayed structure, with one head (further from the bare zone) "less massive" than the other (3), is a misinterpretation of what is actually the interacting head motif seen in side view. The less dense "head" (further from the bare zone) is a projection of the RDs and the denser "head" is a projection of the (larger) MDs in a single motif. The images in *B*, *E*, and *G* were originally published in the *Journal of Structural Biology*. Reprinted from the *Journal of Structural Biology*, 166/2, AL-Khayat, HA, Morris, EP, Squire, JM, The 7-stranded structure of relaxed scallop muscle myosin filaments: Support for a common head configuration in myosin-regulated muscles, 183–194, Copyright (2009), with permission from Elsevier.

1. Vibert P, Craig R (1983) Electron microscopy and image analysis of myosin filaments from scallop striated muscle. *J Mol Biol* 165(2):303–320.
2. AL-Khayat HA, Morris EP, Squire JM (2009) The 7-stranded structure of relaxed scallop muscle myosin filaments: Support for a common head configuration in myosin-regulated muscles. *J Struct Biol* 166(2):183–194, http://www.sciencedirect.com/science/journal/10478477.
3. Vibert P (1992) Helical reconstruction of frozen-hydrated scallop myosin filaments. *J Mol Biol* 223(3):661–671.
4. Zhao FQ, Craig R (2003) Ca^{2+} causes release of myosin heads from the thick filament surface on the milliseconds time scale. *J Mol Biol* 327(1):145–158.
5. Wendt T, Taylor D, Trybus KM, Taylor K (2001) Three-dimensional image reconstruction of dephosphorylated smooth muscle heavy meromyosin reveals asymmetry in the interaction between myosin heads and placement of subfragment 2. *Proc Natl Acad Sci USA* 98(8):4361–4366.

Table S1. Comparison of X-ray patterns of live scallop muscle with averaged Fourier transform of frozen-hydrated scallop thick filaments

Layer line spacing, nm (order)*	Axial spacing, nm (Wray/Millman)†	Axial spacing, nm (this work)	Radial spacings of off-meridional reflections, nm‡ (Wray/Millman)	Radial spacings,‡ nm (this work)
48.0 (3)	48.7/46.4	48.5	NM§/14.3	12.3
20.6 (7)	20.8/20.0	20.5	NM/14.0	10.2
14.4 (10)	14.6/14.5	14.4¶	27.0, 14.5/27.8, 14.3	23.9, 13.1
11.2 (13)	11.2/11.2	11.0	13.0/13.5	12.9
7.25 (20)	7.3/7.26	7.16	36.5, 16.5/35.9, NR‖	31.9, 15.3

This table compares the axial and radial positions of reflections in X-ray diffraction patterns of live scallop muscle with those in the averaged Fourier transform of the frozen hydrated scallop filaments used in this study. Note the excellent agreement between the axial spacings. It is possible that the imperfect correspondence between spacings in the radial direction is due in part to lattice sampling effects in the X-ray pattern that are absent in single filaments (1).

*Nominal layer line spacing in nanometers and order of 144-nm repeat.

†Spacing of reflection measured in X-ray diffraction patterns of live scallop muscle: Wray et al. (2) and Millman et al. (1).

‡Some layer lines have multiple reflections at different radial positions.

§Not measurable in pattern.

¶Assumed. Other spacings are based on this as an internal calibration.

‖Not reported.

1. Millman BM, Bennett PM (1976) Structure of the cross-striated adductor muscle of the scallop. *J Mol Biol* 103(3):439–467.
2. Wray JS, Vibert PJ, Cohen C (1975) Diversity of cross-bridge configurations in invertebrate muscles. *Nature* 257(5527):561–564.

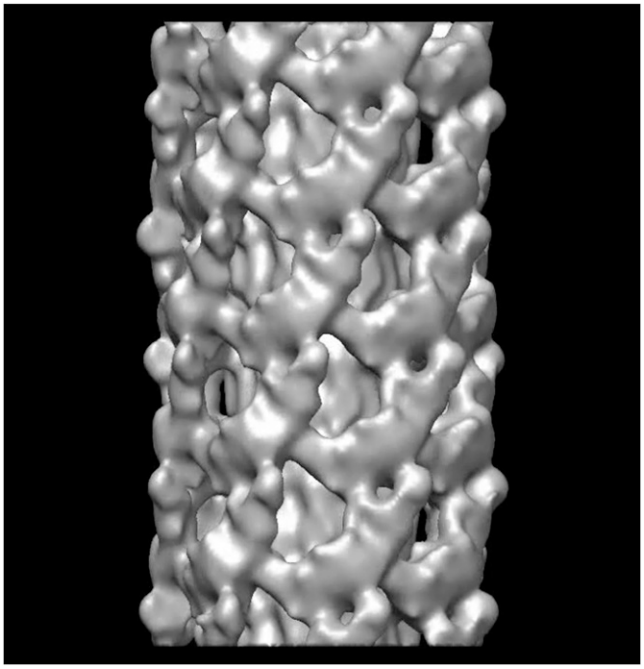

Movie S1. Three-dimensional reconstruction of scallop thick filament rotated about long axis. Reconstruction shows five 14.4-nm levels of sevenfold symmetric crowns of heads lying above the backbone, visible at lower radius (Fig. 2*A*). Five atomic models (ribbon and space-filling representations) have been fitted to show the intermolecular contacts (Fig. 3*A*). Bare zone direction is toward top.

Movie S1

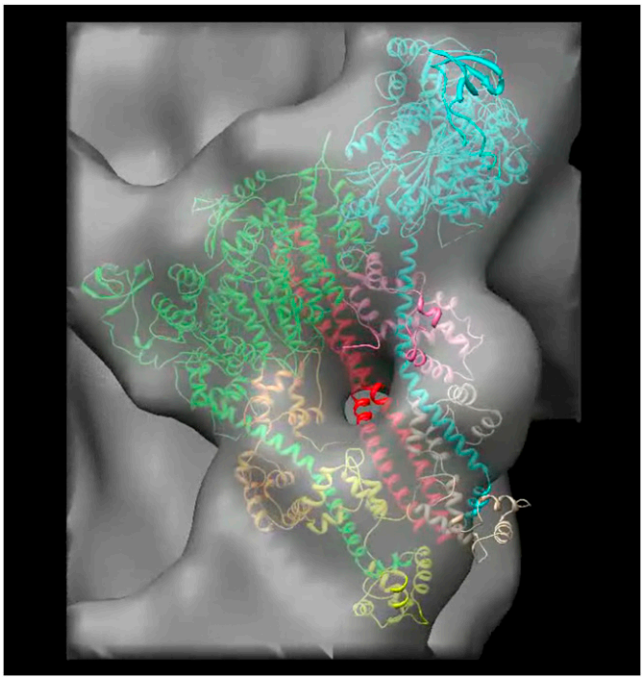

Movie S2. Fitting of ribbon and space-filling atomic models of scallop myosin head domains and S2 to one motif (Fig. 2*B*).

Movie S2

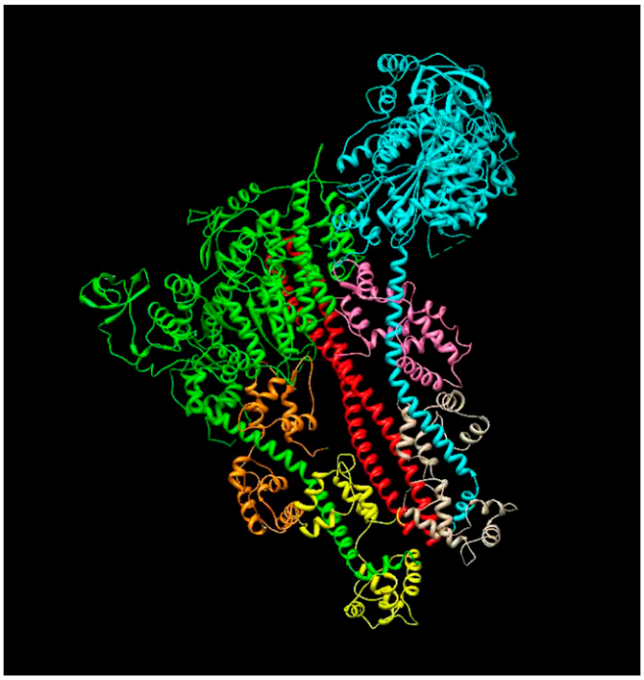

Movie S3. Atomic model of scallop head–head motif. The ribbon and space-filling models were produced by fitting crystallographic models for the scallop motor domain (PDB ID code 1QVI), regulatory domain (PDB ID code 3JTD), and N-terminal fragment of S2 (PDB ID code 3BAS) into the 3D reconstruction (Fig. 2*B*).

Movie S3

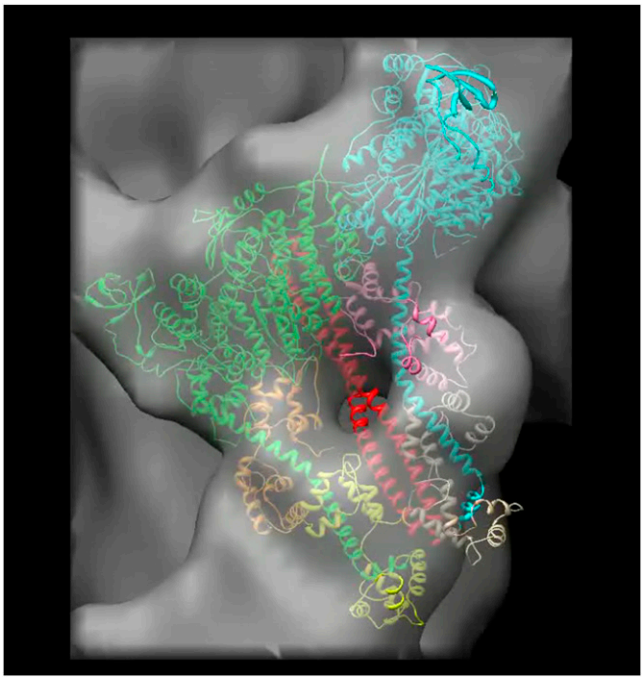

Movie S4. Fit of S2 (ribbon model) to the scallop head–head motif shown at different density contours. The "hole" in the density map between the regulatory domains is filled at lower contours to completely include all of the S2 in this region. The density "gap" between the head–head motif and the filament backbone (as viewed from the bare zone) is bridged at lower contours and shows the path S2 would eventually take to join with the subfilaments.

Movie S4